



Multifunctionalized hydrogels foster hNSC maturation in 3D cultures and neural regeneration in spinal cord injuries

Amanda Marchini^{a,b,1}, Andrea Raspa^{a,1}, Raffaele Pugliese^a, Marina Abd El Malek^b, Valentina Pastori^c, Marzia Lecchi^c, Angelo L. Vescovi^a, and Fabrizio Gelain^{a,b,2}

^aUnità Ingegneria Tissutale, Fondazione Istituto di Ricovero e Cura a Carattere Scientifico Casa Sollievo della Sofferenza, 71013 Foggia, Italy; ^bCenter for Nanomedicine and Tissue Engineering, ASST Ospedale Metropolitan Niguarda, 20162 Milan, Italy; and ^cDepartment of Biotechnology and Biosciences, University of Milano-Bicocca, 20126 Milan, Italy

Edited by Shuguang Zhang, Massachusetts Institute of Technology, Cambridge, MA, and accepted by Editorial Board Member Alan R. Fersht March 6, 2019 (received for review October 29, 2018)

Three-dimensional cell cultures are leading the way to the fabrication of tissue-like constructs useful to developmental biology and pharmaceutical screenings. However, their reproducibility and translational potential have been limited by biomaterial and culture media compositions, as well as cellular sources. We developed a construct comprising synthetic multifunctionalized hydrogels, serum-free media, and densely seeded good manufacturing practice protocol-grade human neural stem cells (hNSC). We tracked hNSC proliferation, differentiation, and maturation into GABAergic, glutamatergic, and cholinergic neurons, showing entangled electrically active neural networks. The neuroregenerative potential of the “engineered tissue” was assessed in spinal cord injuries, where hNSC-derived progenitors and predifferentiated hNSC progeny, embedded in multifunctionalized hydrogels, were implanted. All implants decreased astrogliosis and lowered the immune response, but scaffolds with predifferentiated hNSCs showed higher percentages of neuronal markers, better hNSC engraftment, and improved behavioral recovery. Our hNSC-construct enables the formation of 3D functional neuronal networks in vitro, allowing novel strategies for hNSC therapies in vivo.

3D cell cultures | neural stem cells | self-assembling peptides | spinal cord injury | nervous tissue engineering

Three-dimensional cell culture systems are gaining interest in the scientific community because of the number of potential applications in biotechnology (1). Researchers stimulated induced pluripotent stem cells or embryonic stem cells to self-organize under various conditions to form complex tissue-like structures, recapitulating structural and functional features typical of living tissues, such as absorptive and secretory activities in intestinal and kidney 3D constructs (2, 3). This in vitro technology is also particularly suited for the modeling of diseases with pathological conditions difficult to reproduce in animal experiments and with complex genetics (4–6). In the future, 3D cell constructs may also be used as “patches” for damaged or nonfunctional tissues, favoring a proper engraftment of allogenic cells pretreated in the laboratory (7, 8). A wide variety of 3D constructs have been transplanted in vivo to repair and rescue damaged tissues (9, 10). Usually, the main limitation of these protocols is the use of animal-derived scaffolds like Matrigel as embedding matrices for 3D constructs. Matrigel is derived from decellularized extracellular matrix (ECM) of mouse sarcoma, made of basement membrane components, such as collagens, laminin, and entactin: adhesion proteins enabling excellent cell spreading. However, clinical translation of Matrigel is limited. In addition, limited reproducibility due to the batch-to-batch variation, lack of well-defined composition, and minimal tailorability for different cell/tissue types have to be taken into account for potential applications in the future (11).

To this purpose, synthetic and Nature-inspired biomaterials, such as self-assembling peptides (SAPs), with biophysical and biochemical properties tunable for specific tissues, show better translational potential. Through selected functional motifs and tuned biomechanical properties, SAPs can foster cell attachment, migration, and differentiation in vitro and promote biomaterial–host tissue interactions after implantation (12, 13). A 3D construct densely seeded with entangled nervous cells, with all components suited for clinics, can provide a precious tool for nervous repair, but such configuration with SAP-based biomaterials has not yet been achieved. An optimized SAP-based 3D construct could be both a standardized 3D in vitro model, but also a potential carrier of pretreated cells coaxing their engraftment in vivo. For example, designed 3D SAP systems with densely seeded neural cells can prompt the development of standardized nervous tissue models in vitro but also tackle diseases of the CNS, such as—but not limited to—spinal cord injury

Significance

Cells reside in 3D microenvironments in living tissues; consequently, 3D cultures gained great interest because they better mimic the natural conditions of cells. Self-assembling peptides (SAPs) are synthetic bioabsorbable biomaterials that can provide customized 3D microenvironments regulating cell functionalities and tissue repair. Here we introduce a SAP-hydrogel designed to support human neural stem cell (hNSC) differentiation in 3D serum-free conditions, generating mature and active human neurons in vitro. We also demonstrate its functional neuroregenerative potential in rat spinal cord injuries, peaking when seeded with hNSCs progeny predifferentiated in vitro for 6 weeks. Despite these promising results, this approach should be confirmed in the future with medium-size animal models and with additional and refined behavioral tests before entering a clinical trial.

Author contributions: A.M., A.R., and F.G. designed research; A.M., A.R., R.P., M.A.E.M., V.P., M.L., and F.G. performed research; A.L.V. contributed new reagents/analytic tools; A.M., A.R., R.P., V.P., M.L., A.L.V., and F.G. analyzed data; and A.M., A.R., M.L., and F.G. wrote the paper.

Conflict of interest statement: F.G. and A.L.V. are inventors on the patent US9,273,101B2 “Functionalized biomaterials for tissue regeneration.” All other authors declare no competing interests.

This article is a PNAS Direct Submission. S.Z. is a guest editor invited by the Editorial Board.

This open access article is distributed under [Creative Commons Attribution-NonCommercial-NoDerivatives License 4.0 \(CC BY-NC-ND\)](https://creativecommons.org/licenses/by-nc-nd/4.0/).

¹A.M. and A.R. contributed equally to this work.

²To whom correspondence should be addressed. Email: f.gelain@css-mendel.it.

This article contains supporting information online at www.pnas.org/lookup/suppl/doi:10.1073/pnas.1818392116/-DCSupplemental.

Published online March 28, 2019.

(SCI). Current medical treatments for SCI are limited by inhibitory factors located in both the cyst cavity and fibroglial scar, typical outcomes of subacute and chronic SCI (14–16). Several strategies, including cellular-based therapies, have been used to promote regeneration of injured axons (17, 18). Despite many efforts with different cell types, fate of transplanted cells has been typically poorly controlled (19). Indeed, authors agree on the idea that guiding cell fate prior to and after transplantation may be the key to success (20–22). Among these approaches, SAPs can be used as scaffolds providing biomimetic microenvironments tuning the differentiation and favoring the engraftment of cellular transplants (23–27).

In this work we developed a serum-free nanostructured construct, dubbed HYDROSAP, to introduce a 3D *in vitro* model of densely cultured human neural stem cell (hNSCs), hNSC-HYDROSAP, assessing its neuroregenerative potential into a subacute hemisection model of SCI. Aiming at the development of a system with minimal translational hurdles, a synthetic SAP-based scaffold, made of functionalized linear SAPs and branched SAPs (28, 29), was optimized for long-term *in vitro* cell cultures. Embedded hNSCs were assessed for their proliferation, differentiation, and maturation. Immunophenotyping revealed neurons expressing GABAergic, glutamatergic, and cholinergic markers, with concomitant decreased expression of immature markers. Furthermore, electrophysiological tests confirmed the presence of electrically active neurons. Tackling the issue of proper differentiation of hNSC transplants, we implanted hNSC-HYDROSAP at two levels of maturation (hNSC-derived progenitors and hNSC progeny predifferentiated *in vitro* for 6 wk) in subacute SCI. In all cases, hNSC-HYDROSAP implants reduced inflammation and astrogliosis, leading to significant improvements in axon regeneration and motor functional recovery. Furthermore, predifferentiating hNSC *in vitro* prior to implantation increased the presence of transplanted stem cell progeny expressing markers for phosphorylated neurofilaments, GABAergic and glutamatergic neurons. Therefore, the newly characterized *in vitro* model of entangled 3D neuronal networks cells may also be a useful tool to better control stem cell differentiation in future therapies.

Results

HYDROSAP 3D Culture Systems Foster hNSC Spreading and Formation of Entangled Cellular Networks in Long-Term Cultures. We developed hNSC-HYDROSAP to obtain long-term cultures of densely seeded hNSCs in 3D biomimetic microenvironments. pureHYDROSAP is composed by multifunctionalized SAPs and branched SAPs selected from previously published works (13, 28, 29), where NSCs have been used as target of phage-display panning and for cytotoxicity assessments. Sucrose and sodium hydroxide (NaOH) solutions were also used to increase, respectively, osmotic pressure and pH to more physiological values than in pure-HYDROSAP. Furthermore, tuning of the specific molar ratio of the different peptide species, and of the total SAP concentration, was conducted to provide maximum functional motif efficacy (30) and biomechanical properties of the substrate, enabling optimal hNSC survival and differentiation (31), falling in the range of nervous tissues (100–1,000 Pa) (32). When the resulting mixture was exposed to culture medium, hNSC-HYDROSAP self-assembled into stable disk-like scaffolds made of nanofibrous β -rich structures featuring solid-like behavior and stiffness falling in the range of nervous tissues (29, 33) (*SI Appendix, Fig. S1*). Aiming at creating a heavily entangled network of differentiating neural cells, we selected 4.5×10^4 cells/ μ L as optimal seeded cell density for hNSC-HYDROSAP constructs, yielding to a total of 1.8×10^6 seeded cells per 0.5-cm-wide construct. hNSC-HYDROSAP was tested at different time points *in vitro*: at 0 d *in vitro* (DIV) [hNSC-HYDROSAP(T0)]—that is, 1 h after seeding—with the highest percentage of stem cells (33); and at 1 DIV [hNSC-HYDROSAP(1D)], when the medium depleted of epidermal growth factor (EGF) initiated the

differentiation process of hNSCs; at subsequent weeks (from 1 to 10), when NSC differentiation proceeded toward mature phenotypes [favored by supplementing culture media with brain-derived neurotrophic factor (BDNF) and leukemia inhibitory factor (LIF) at 2 DIV]. In these serum-free long-term cultures, hNSC-HYDROSAP was analyzed by whole-cell patch-clamp recordings and characterized by immunofluorescence analyses. Eventually, hNSC-HYDROSAP(6W) (6 wk) and hNSC-HYDROSAP(1D) constructs were selected for *in vivo* studies (SCI rat model). A schematic representation of the above-mentioned experimental protocol is depicted in Fig. 1*A*. Free-floating discs of hNSC-HYDROSAPs (Fig. 1*B*) showed standard round-shaped hNSCs at 1 DIV and entangled cellular structures at 6 wk (H&E-stained sections in Fig. 1*B*).

HYDROSAP Enables hNSC Survival in Long-Term Serum-Free Cultures.

hNSC-HYDROSAP was analyzed from 1 DIV to 10 wk by immunostaining to assess cell viability, proliferative state, and stemness maintenance. To evaluate the initial cell condition, the T0 sample was tested 1 h after seeding (dotted lines in graphs in Fig. 1*C–G*). Because T0 results showed comparable values to hNSC-HYDROSAP(1D), T0 is hereafter not mentioned. Percentages of dead cells, evaluated through Tunel assay, were $10.84 \pm 0.94\%$ at 1 DIV; apoptotic values increased at 1 wk but were significantly higher than 1 d only at 8 and 10 wk ($28.47 \pm 3.79\%$, $*P < 0.05$; $32.8 \pm 3.22\%$, $**P < 0.01$, respectively) (Fig. 1*C* and *D*). At 1 d Ki67, nuclear proliferative marker, was $15.17 \pm 0.49\%$ (Fig. 1*E* and *F*), while at 4 wk it decreased to $3.38 \pm 1.46\%$ ($**P < 0.01$), a percentage value maintained in 6-, 8-, and 10-wk samples (1 d vs. 6 wk $***P < 0.001$, 1 d vs. 8 and 10 wk $**P < 0.01$). Similarly, Nestin⁺ cells were significantly the highest in both 1-d and 1-wk samples ($***P < 0.001$) (Fig. 1*G* and *H*). The same strategy was adopted to analyze hNSCs encapsulated in CULTREX-BME, used as a positive control (CULTREX 3D), and maintained in culture from 1 to 8 wk (*SI Appendix, Fig. S2*). CULTREX-BME is a valid *in vitro* ECM-like matrix (31) but with limited application in clinics (34). CULTREX 3D showed significant lower percentage of apoptotic cells (*SI Appendix, Fig. S2 A and B*) if compared with results obtained for hNSC-HYDROSAP (*SI Appendix, Table S1*). On the other hand, percentage of Ki67⁺ cells were similar to hNSC-HYDROSAP at 1 d and 1 wk but they sharply decreased at 2 wk (*SI Appendix, Fig. S2 C and D* and *Table S2*). Finally, percentages of Nestin⁺ cells were similar in both hNSC-HYDROSAP and CULTREX 3D without significant differences (*SI Appendix, Fig. S2 E and F* and *Table S3*).

HYDROSAP Induces Neural Phenotype Differentiation in Encapsulated hNSCs.

The capability of hNSCs embedded in a 3D culture system to differentiate into the three main phenotypes of neural tissue was evaluated by immunocytochemical stainings (Fig. 2*A* and *B*). A small fraction of seeded cells was found positive for the tested markers in the 1-d sample: $11.3 \pm 1.4\%$ of encapsulated hNSCs were positive for GFAP, a marker for astrocytes. At 1 wk, GFAP expression significantly increased and plateaued until 10 wk ($***P < 0.001$). Additionally, GALC-O4⁺ cells were not at 1 d, but they showed up at 1 wk ($18.0 \pm 2.63\%$), with similar values at all subsequent timepoints. Finally, β III-TUB, an immature neuronal marker, appeared since 1 DIV but revealed a more than threefold increment after 1 wk (1 d $6.31 \pm 1.28\%$ vs. 1 wk $22.56 \pm 1.96\%$, $***P < 0.001$). Moreover, positive cells for β III-TUB and GFAP markers were evenly distributed inside the construct, from the edges to the core, as could be seen in full-coronal sections of Fig. 2*C*. In CULTREX 3D, similar percentages of GFAP and β III-TUB⁺ cells were detected, but values of GALC-O4 were higher than in hNSC-HYDROSAP at 1 d and 8 wk (*SI Appendix, Fig. S3 A and B* and *Tables S4–S6*).

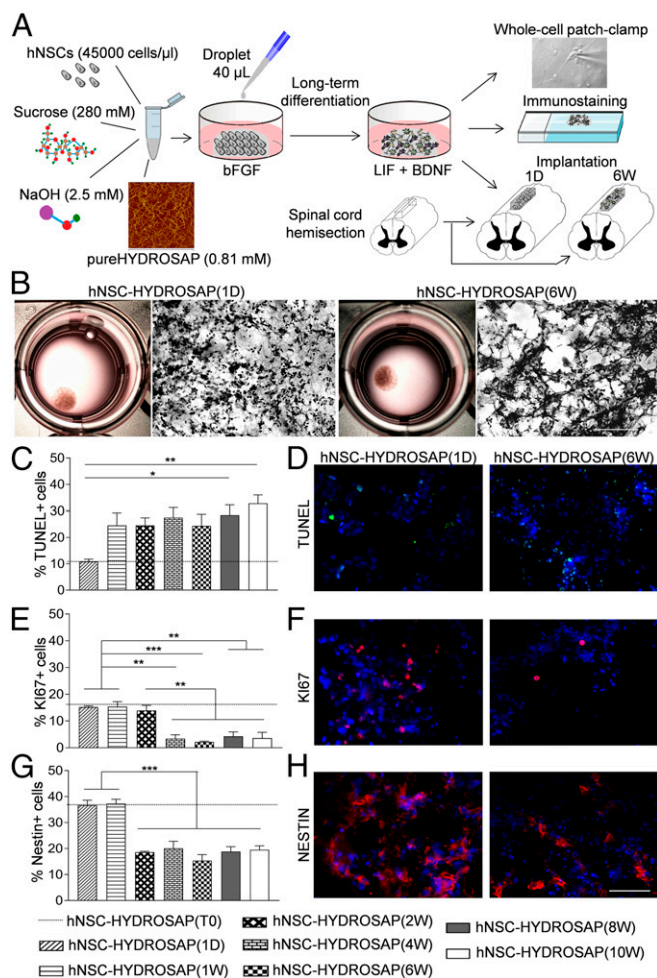


Fig. 1. Design and 3D cell cultures characterization of hNSC-HYDROSAP. (A) Schematic illustration of overall protocol adopted to prepare hNSC-HYDROSAP, comprising pureHYDROSAP, hNSCs, NaOH, and sucrose solution. Details are described in *SI Appendix*. A droplet of 40 μ L was placed in 24-wells plates with serum-free medium supplemented with bFGF and, subsequently, shifted to a medium with LIF and BDNF supplements. hNSC-HYDROSAP was maintained in culture for the following time points: 0 d (T0 sample), 1 d (1D), and 1, 2, 4, 6, 8, and 10 wk. Three-dimensional cell culture characterization was performed through whole-cell patch-clamp recording for electrophysiological analysis (Top) and immunocytochemical analysis assessing cell apoptosis, proliferation, differentiation, and maturation (Middle). Finally, HYDROSAP alone and two selected hNSC-HYDROSAPs constructs [at 1 DIV, hNSC-HYDROSAP(1D), and at 6 wk, hNSC-HYDROSAP(6W)] were implanted in a rat SCI model (Bottom). (B) Representative images of whole hNSC-HYDROSAP(1D) (Left) and hNSC-HYDROSAP(6W) (Right) constructs and their respective H&E stainings. A more entangled network of cells can be seen at 6 wk in culture. (Scale bar, 100 μ m). (C, E, and G) Time-tracking of cells positive for TUNEL assay (C), Ki67 (E), and Nestin markers (G) reveal decreased cell viability, proliferation, and stemness over time. All graphs show mean \pm SEM of triplicate experiments. Statistical analysis showed significant differences ($*P < 0.05$; $**P < 0.01$; $***P < 0.001$) using one-way ANOVA analysis of variance followed by Tukey posttest. Dotted lines represent values of positive cells in hNSC-HYDROSAP at T0. (D, F, and H) Fluorescence images of hNSCs progenies in hNSC-HYDROSAP(1D) (Left) and hNSC-HYDROSAP(6W) (Right) positive for TUNEL (D, green), Ki67 (F, red), and Nestin (H, red) markers. Cell nuclei are counterstained with DAPI (blue). (Scale bar, 50 μ m).

hNSC-HYDROSAPs Constructs Express Markers of GABAergic, Glutamatergic, and Cholinergic Neurons in Vitro. Neuronal network development and maturation in hNSC-HYDROSAP was assessed for up to 10 wk. We analyzed the expression of neuronal markers like GAP43 (growth-cones associated protein), MAP2 (microtubule-associated protein 2), and SMI31 (phosphorylated neurofilament protein).

Furthermore, GABA and VGLUT1 markers were evaluated to detect inhibitory and excitatory neurons, respectively (Fig. 2D). MAP2 is a neuron-specific cytoskeletal protein used as a marker of neuronal phenotype. In 6- and 8-wk samples, MAP2 expression significantly increased if compared with 1 wk (1 wk $14.76 \pm 1.02\%$ vs. 6 wk $26.44 \pm 3.4\%$, $**P < 0.01$; 1 wk vs. 8 wk $24.77 \pm 0.77\%$, $*P < 0.05$); representative images of 1 and 6 wk are shown in Fig. 2E. In the same way, cells positive for GAP43, a membrane-associated phosphoprotein marker mainly expressed in elongating axons, were higher in 4-wk ($35.23 \pm 1.46\%$) and 6-wk ($33.48 \pm 0.78\%$) samples than in 1 wk ($22.5 \pm 3.18\%$), 8 wk ($25.35 \pm 2.41\%$), and 10 wk ($21.93 \pm 0.62\%$) (Fig. 2D and E). Interestingly, no significant differences were observed over time for phosphorylated neurofilaments marked by SMI31 ($\sim 21\%$) and for GABAergic neurons ($\sim 23\%$). Whole-construct transversal sections (Fig. 2F) showed good distribution of GABA⁺ cells within HYDROSAP (spaces inside construct are due to cryo-sectioning). Instead, VGLUT1⁺ cells increased over time, peaking with a twofold increment in both hNSC-HYDROSAP(8W) ($22.42 \pm 2.87\%$) and hNSC-HYDROSAP(10W) ($21.43 \pm 3.11\%$) if compared with hNSC-HYDROSAP(1W) ($11.38 \pm 2.53\%$) (1 wk vs. 8 wk $**P < 0.01$; 1 wk vs. 10 wk $*P < 0.05$) (Fig. 2D and E). Choline acetyltransferase (ChAT), similarly to GABA and VGLUT1, was detected from 1 wk in vitro until the end of the experiments (Fig. 3A). Colocalization of MAP2 mature neurons and ChAT⁺ cells was also present (white arrows in Fig. 3B). Additionally, expression of myelin basic protein (MBP), a marker for myelin sheaths surrounding myelinated axons in vivo, was detected from 4 wk on (Fig. 3A). Representative confocal images in Fig. 3C show GABA⁺ cells with no MBP-positivity in hNSC-HYDROSAP(1W), and an extensive network of GABA⁺ cells intermingled with expression of MBP in hNSC-HYDROSAP(6W). GAP43⁺ and GABA⁺ cells showed similar values in hNSC-HYDROSAP and CULTREX 3D throughout the experimental time frame, while MAP2 and SMI31 values were higher in CULTREX 3D at 1 wk only (*SI Appendix*, Fig. S3C and D and Tables S7–S10); finally, VGLUT1⁺ cells were statistically lower in CULTREX 3D than in hNSC-HYDROSAP (*SI Appendix*, Table S11). Notwithstanding the above-mentioned differences, hNSC differentiation in both substrates was similar. Representative images for CULTREX 3D (1 wk) and CULTREX 3D (6 wk) are shown in *SI Appendix*, Fig. S3C.

Electrophysiological Analysis in Vitro Reveals Electrically Active Neurons.

To assess whether cells in hNSC-HYDROSAP were electrically active, functional analyses at the single-cell level were performed. Cells that morphologically resembled mature neurons (Fig. 1A) were investigated by patch-clamp technique in the whole-cell configuration. When recording in the voltage-clamp mode, neuron-like cells exhibited inactivating inward and outward currents, which were compatible with the opening of voltage-dependent sodium and potassium channels, respectively (Fig. 4A). Potassium current expression did not change significantly through the weeks in culture: it was detected in 100% of the tested cells, but the peak current increased significantly from 2 to 4 wk and remained significantly larger also at 6, 8, and 10 wk (Fig. 4B and Table 1). In contrast, the percentage of cells endowed with sodium currents significantly increased from 44% at 2 wk to 100% at 4 wk (χ^2 test, $**P < 0.01$), and remained at $\sim 100\%$ in the following samples (Table 1). Moreover, average sodium current peak increased from 145 ± 80 pA at 2 wk to 649 ± 162 pA at 4wk (current density: 9.8 ± 3.7 pA/pF at 2 wk, 26.1 ± 5.9 at 4 wk) and it remained stable until 10 wk in culture (Fig. 4B and C and Table 1). Changes in sodium current expression and density in hNSC-HYDROSAP (4–10 wk) suggested a maturation of the electrophysiological properties (Fig. 4D and E). In fact, the trend of the results obtained in the current-clamp mode at 6 wk was consistent with a more mature neuronal phenotype (but with no significant difference among the timepoints), when resting membrane potential (V_{rest}) reached more hyperpolarized values

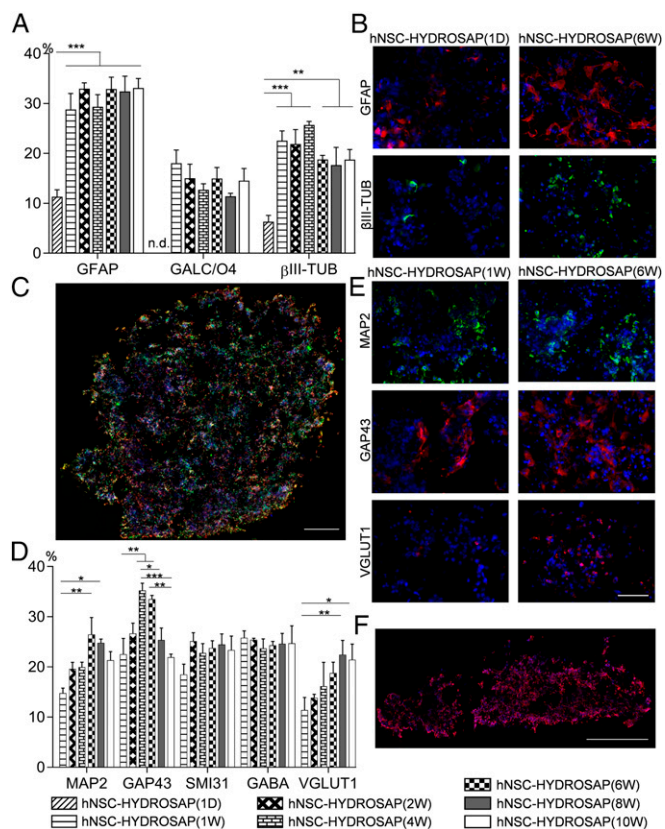


Fig. 2. Neural differentiation and neuronal maturation in 3D cell cultures at different time points. (A) Quantification of differentiated hNSCs encapsulated in HYDROSAP at 1 d and 1, 2, 4, 6, 8, and 10 wk. Percentages of GFAP⁺ (astrocytes), GALC/O4⁺ (oligodendrocytes), and βIII-TUB⁺ (neurons) cells are shown. GALC/O4⁺ cells were not detected (n.d.) at 1 DIV. Significant differences (** $P < 0.01$ and *** $P < 0.001$) were noticed over time for GFAP and βIII-TUB markers compared with hNSC-HYDROSAP(1D). (B) Immunostaining for GFAP (red) and βIII-TUB (green) markers of hNSC-HYDROSAP(1D) (Left) and of hNSC-HYDROSAP(6W) (Right). A more entangled network of positive cells can be seen at 6 wk in culture. (C) Image of full coronal section after immunostaining for βIII-TUB (green) and GFAP (red). (D) Quantitative evaluation of general mature neuronal markers (MAP2, GAP43, and SMI31), of GABAergic (GABA) and glutamatergic (VGLUT1) neurons. SMI31 and GABA expression remained approximately constant throughout the experiments, while MAP2, GAP43, and VGLUT1 expression increased and peaked at 6–8 wk (** $P < 0.05$; *** $P < 0.01$; * $P < 0.001$). (E) Representative fluorescence images of hNSC-HYDROSAP(1W) and hNSC-HYDROSAP(6W) for MAP2 (green, Top), GAP43 (red, Middle), and VGLUT1 (red, Bottom) mature markers. (F) Distribution of GABA⁺ cells (red) in transversal section. Cell nuclei are stained with DAPI (blue). All graphs show mean \pm SEM of triplicate samples per each time point. Significant differences were detected by two-way ANOVA analysis followed by Tukey's multiple-comparison test. (Scale bars, 50 μ m in B and E; 500 μ m in C and F.)

[-62 ± 4 mV for hNSC-HYDROSAP(6W) vs. -47 ± 6 mV for hNSC-HYDROSAP(2W)] (Fig. 4D), and the percentage of neurons able to generate action potentials (AP) reached $\sim 20\%$ in hNSC-HYDROSAP(6W) (Fig. 4E). APs were evoked by injecting depolarizing current pulses by the patch electrode. Among cells showing evoked APs, the large majority (86%) generated only one AP > 0 mV, while firing of multiple APs was recorded in 14% (Fig. 4F). Similar to hNSC-HYDROSAP, CULTREX 3D cultures reached maturation at 6 wk, with 18% of total cells able to generate APs. However, significant changes in sodium and potassium currents in CULTREX 3D cultures were not observed. (SI Appendix, Fig. S4 and Table S12).

hNSC-HYDROSAP Can Be Used as a Carrier for hNSC-Differentiated Progeny Transplants in SCI. Inspired by the results of the in vitro characterization, we weighted the translational potential of the

tested in vitro model made of good manufacturing practice protocol (GMP)-grade hNSCs cultured in serum-free media and synthetic biomimetic hydrogels. For the assessment of the neuroregenerative potential of our constructs in vivo, we selected a dorsal hemisection model (T9–T10) of SCI in rats, characterized by severe axonal damage, associated with motor and sensory function loss caudal to the injury, and by limited spontaneous recovery (35). Because a good amount of research raised concerns about lack of appropriate NSC transplant differentiation and engraftment in vivo (36–38), we wondered if providing biomimetic microenvironments embedding hNSCs in vivo, or predifferentiating the stem cell population in vitro before transplantation would help in this issue. To address both options, we selected respectively hNSC-HYDROSAP(1D) and hNSC-HYDROSAP(6W). hNSC-HYDROSAP(6W) was chosen because best results were obtained at 6 wk in vitro in terms of cell viability and differentiation. Control groups were pureHYDROSAP and sham-operated animals (SHAM).

HYDROSAP Implants Ameliorate Behavioral Recovery in SCI. Hindlimb locomotor function recovery was evaluated by an open-field Basso, Beattie and Bresnahan (BBB) test. BBB scoring results at each time point are depicted in Fig. 5. All animals confirmed normal motor function before injury (BBB score = 21), with a significant drop after dorsal hemisection, characterized by a slight movement of one or two joints (average BBB score = 1.58). In the weeks following implantation surgery, the hNSC-HYDROSAP(6W) group showed the highest BBB scores. Statistically significant differences between hNSC-HYDROSAP(6W) and SHAM groups were seen at 21 d (6.0 ± 0.4 vs. 3.0 ± 0.68), 24 d (6.6 ± 0.4 vs. 4.1 ± 0.67), and 28 d (6.7 ± 0.4 vs. 4.1 ± 0.71) after injury (* $P < 0.05$, $n = 5$). Interestingly, at 31 and 35 d the BBB score of

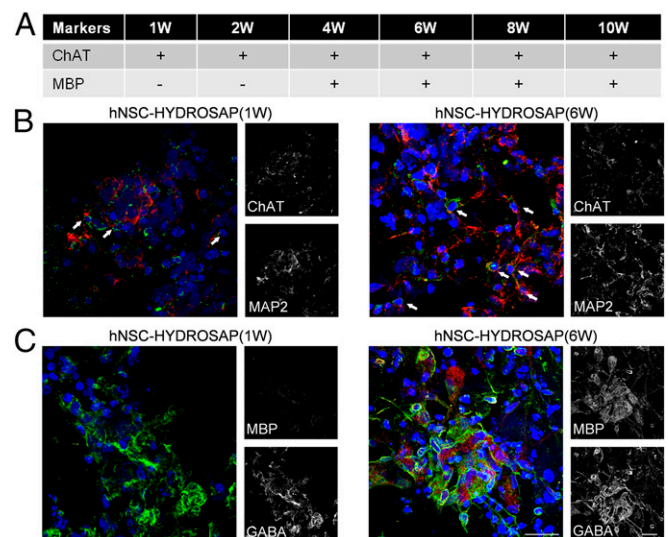


Fig. 3. ChAT and MBP markers expression in 3D cell cultures. (A) Table represents expression (+) or absence (–) of ChAT and MBP markers in hNSC-HYDROSAP constructs at different time points. Analysis was performed in triplicate through a Nikon A1 confocal microscope. Marker expression (or its absence) has been verified on three different samples per each experimental group. (B) Colocalization of mature (MAP2 in red), and cholinergic (ChAT in green), neurons for hNSC-HYDROSAP(1W) (Left) and hNSC-HYDROSAP(6W) (Right). White arrows point at signal colocalization. (C) Confocal image confirmed absence of MBP (red) in hNSC-HYDROSAP(1W) (Left column) and its expression in hNSC-HYDROSAP(6W) (Right column). GABAergic neurons are stained with GABA marker (green). A more entangled and mature morphology of positive neuronal cells could be appreciated in hNSC-HYDROSAP(6W). Cell nuclei are labeled with DAPI (blue). (Scale bars, 20 μ m in B and C.)

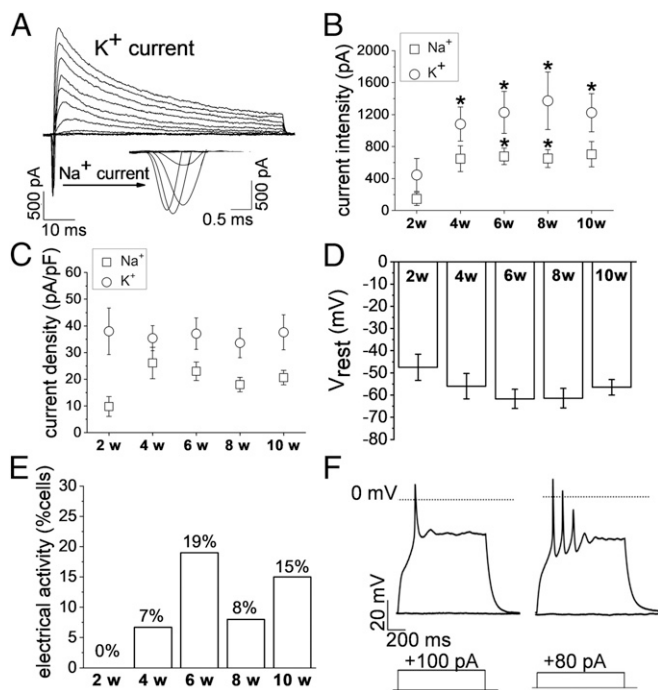


Fig. 4. Electrophysiological properties of hNSC-HYDROSAP-derived neurons at different time-points in 3D cell cultures. (A) Record of sodium and potassium currents through voltage-dependent channels, evoked by membrane depolarization from a holding potential of -90 mV. Tested potentials ranged from -80 to $+20$ mV. (B) Increment of sodium and potassium current amplitude through the weeks of culture [compared with 2 wk ($*P < 0.05$)]. (C) Mean sodium and potassium current densities detected at the different weeks of culture. (D) Resting membrane potential (V_{rest}) hyperpolarization trend over time. (E) Increasing percentage of cells endowed with electrical activity through the tested weeks of culture. (F) Representative responses induced by current steps injected through the patch electrode. In the majority of active cells only one AP ≥ 0 mV could be generated at 4, 6, 8, and 10 wk in culture (Right). Multiple APs (Left) were recorded anyway, but their presence could not be correlated with weeks of culture. The dotted line in the traces represent the level of 0 mV. In both the representative traces, APs were evoked from resting membrane potential by depolarizing currents depicted below each trace ($+100$ pA and $+80$ pA, respectively).

hNSC-HYDROSAP(6W) further increased (7.2 ± 0.5 and 7.7 ± 0.7 , respectively) and plateaued until the end of experiments. A similar significant trend was observed in HYDROSAP in respect to SHAM from 38 d (6.7 ± 0.45 vs. 3.7 ± 0.89) after injury ($*P < 0.05$, $n = 5$). As shown in Fig. 5, the treatment with hNSC-HYDROSAP(1D) also led to an amelioration of hindlimb motor functions. For hNSC-HYDROSAP(1D) significant improvements compared with SHAM group were found at 52 d (5.6 ± 0.85 vs. 2.8 ± 0.87), 56 d (5.5 ± 0.9 vs. 2.5 ± 0.86), and 59 d (5.8 ± 0.89 vs. 2.9 ± 0.9) after

injury ($*P < 0.05$, $n = 5$). However, no significant differences between HYDROSAP and hNSC-HYDROSAP groups were seen, while a few favorable ones for hNSC-HYDROSAP(6W) were detected in respect to hNSC-HYDROSAP(1D) (SI Appendix, Table S13). Body-weight changes are presented in SI Appendix, Fig. S54. All rats showed a decreased body weight at 1 wk, as expected, immediately after injury. However, correlation analysis showed a linear relationship between body weight gain vs. BBB score improvements (SI Appendix, Fig. S5B). Treadmill tests began at 3 d after injury (see Materials and Methods for details); we collected the overall distance (meters) walked by each rat. After the initial impairment detected right after injury and subsequent implantation treatment, all experimental groups increased their average total walked distance: while HYDROSAP plateaued to highest values in less time, no significant difference was found among the treated groups at any timepoint. (SI Appendix, Fig. S5C). Here too, a positive correlation was found between treadmill test values and BBB score (SI Appendix, Fig. S5B).

HYDROSAP-Encapsulated hNSCs Engraft and Differentiate in Vivo.

Animals were euthanized 2 mo after treatment and histological analyses were performed to characterize host-tissue response to the implanted 3D cellular constructs and, if any, neural regeneration occurred in experimental groups that had previously featured significant functional recovery. To test the neuro-regenerative potential of HYDROSAP on SCI, we chose a subacute spinal cord model: treatment was performed at 7 d after lesion. In addition, to track transplanted cells engraftment, hNSCs were previously tagged with PKH26 dye prior encapsulation into HYDROSAP and subsequent culturing in vitro. Immunostaining using the nuclear marker Hoechst revealed presence of PKH26⁺ cells in all animals of hNSC-HYDROSAP(1D) and hNSC-HYDROSAP(6W) groups at 8 wk posttransplant, mainly located in the implantation site: average total counted PKH26⁺ cells in both groups were $7,513 \pm 788.5$ and $8,417 \pm 901.4$ cells per animal, respectively (no significant difference, $P = 0.44$) (Fig. 6A). While a small fraction of PKH26 cells still expressed the proliferation marker KI67 (1 d $3.26 \pm 0.82\%$, 6 wk $2.63 \pm 0.62\%$; $P = 0.56$) at 8 wk posttransplant, higher percentage values showed cellular apoptosis (Tunel), and macrophage-mediated (CD68), as well as microglial phagocytoses (IBA) of transplanted cells (Fig. 6B and SI Appendix, Fig. S64). As to glial differentiation PKH26⁺ cells expressed, in both hNSC-HYDROSAP(1D) and hNSC-HYDROSAP(6W) groups, a similar percentages of GFAP⁺ (astrocytes) ($12.73 \pm 3.64\%$ and $11.68 \pm 2.11\%$) and MBP⁺ (myelin) ($12.24 \pm 3.24\%$ and $13.12 \pm 4.33\%$) (Fig. 6B and C) cells. Among PKH26⁺ cells, higher values were obtained for markers associated with neuronal phenotypes (β III-TUB, GAP43, SMI31, GABA, and VGLUT1) (Fig. 6D), being the highest for hNSC-HYDROSAP(6W) in the case of markers for mature neurons (SMI31: 1 d $8.32 \pm 0.84\%$ and 6 wk $12.18 \pm 1.05\%$, $*P < 0.05$; GABA: 1 d $10.1 \pm 1.13\%$ and 6 wk $20.45 \pm 1.10\%$, $***P < 0.001$; VGLUT1: 1 d $6.32 \pm 0.50\%$ and 6 wk $15.66 \pm 2.84\%$, $*P < 0.05$) (Fig. 6D and E). On the other hand, the

Table 1. Electrophysiological properties of neurons in hNSC-HYDROSAP 3D cultures, recorded by the patch-clamp technique

Weeks in culture	No. of cells	Capacity (pF)	V_{rest} (mV)	I_{Na} (pA)	I_{Na} density (pA/pF)	Cells with I_{Na} (%)	I_K (pA)	I_K density (pA/pF)	Cells with I_K (%)	Cells with AP (%)
2	9	10 ± 3	-47 ± 6	145 ± 80	10 ± 4	44	445 ± 207	38 ± 9	100	0
4	17	31 ± 5	-56 ± 6	649 ± 162	26 ± 6	100**	$1,081 \pm 213^*$	35 ± 5	100	7
6	17	31 ± 4	-62 ± 4	$677 \pm 102^*$	23 ± 3	100**	$1,227 \pm 263^*$	37 ± 6	100	19
8	13	35 ± 5	-61 ± 4	$651 \pm 111^*$	18 ± 3	92*	$1,373 \pm 361^*$	34 ± 5	100	8
10	13	34 ± 5	-56 ± 3	704 ± 158	21 ± 3	100**	$1,224 \pm 238^*$	38 ± 7	100	15

Significantly larger sodium (I_{Na}) and potassium (I_K) currents were observed, respectively, in 6- and 8-wk, and in 4-, 6-, 8-, and 10-wk samples compared with 2 wk. Also, significantly higher percentages of cells expressing sodium current were observed in 4-, 6-, 8-, and 10-wk samples compared with 2 wk ($*P < 0.05$ and $**P < 0.01$).

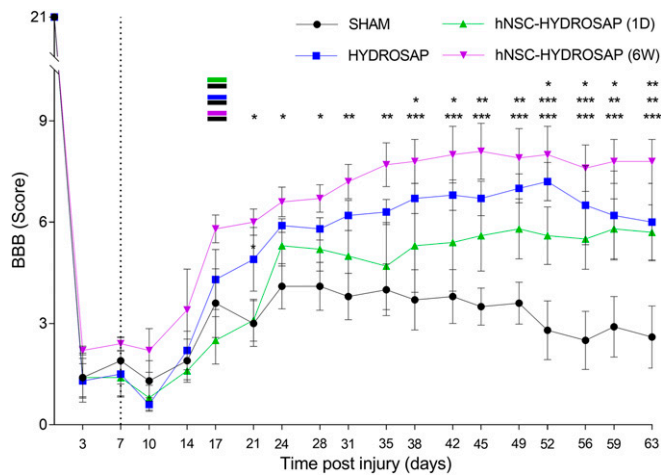


Fig. 5. Behavioral recovery analyses after HYDROSAP implantation in SCI. BBB scores were performed for SHAM (black), HYDROSAP (blue), hNSC-HYDROSAP(1D) (green), and hNSC-HYDROSAP(6W) (magenta) experimental groups. Dotted line outlines the day of implantation (1 wk after injury). All rats showed a slight natural recovery until ~21 d after dorsal hemisection of spinal cord. Rats with hNSC-HYDROSAP(6W) showed a statistically significant increased BBB score after 21 d, compared with SHAM, until the end of the experiment (magenta–black indication). A comparable significant trend was observed in HYDROSAP group since 38 d (blue–black indication for HYDROSAP and SHAM). A significant improvement in hNSC-HYDROSAP(1D) was found since 52 d [green–black indication for hNSC-HYDROSAP(1D) and SHAM]. Data are presented as mean \pm SEM, two-way ANOVA with Tukey post hoc test evaluated statistical differences among the four groups over time ($n = 5$ per group; * $P < 0.05$, ** $P < 0.01$, *** $P < 0.001$).

ratio of PKH26⁺ cells expressing β III-TUB and GAP43 markers was similar in both groups. While β III-TUB⁺ cells showed a more mature morphology after engraftment in vivo than in hNSC-HYDROSAP (6W) in vitro, transplanted GAP43⁺ cells showed similar neurite outgrowth to 6 wk in vitro.

Gliotic Scar Formation and Macrophage Infiltration Are Reduced in Treated Groups. At 8 wk after treatment, lesion epicenter tissues were processed (*Materials and Methods*) to quantify the presence of unsaturated chondroitin sulfate proteoglycans (CSPGs) disaccharides involved in ECM remodeling in SCI (39). We detected abundant values of unsaturated sugar chains in hNSC-HYDROSAP(1D) and hNSC-HYDROSAP(6W) groups in comparison with HYDROSAP and SHAM groups (SHAM vs. 1 d *** $P < 0.001$; SHAM vs. 6 wk ** $P < 0.01$; HYDROSAP vs. 1 d ** $P < 0.01$) (Fig. 7A), being the highest in hNSC-HYDROSAP(1D). HYDROSAP also showed higher values of unsaturated CSPGs in respect to SHAM but with no statistically significant difference. ECM remodeling results were also matched by GFAP marker expression analyses. GFAP immunoreactivity (see *Materials and Methods* for details), assessing the effect of scaffold implantation over gliosis, showed reactive astrogliosis in the host tissue surrounding the lesions: GFAP formed a broader glial border in the SHAM group, compared with lower values in treated groups (SHAM vs. HYDROSAP * $P < 0.05$; SHAM vs. 1 d ** $P < 0.01$) (Fig. 7B and C). In addition, GFAP expression showed the most significant differences between SHAM and treated groups caudally to the lesions (Fig. 7D). Moreover, the quantified area reactive to CD68, a transmembrane glycoprotein highly expressed in monocytes and macrophages, was reduced in all treated groups, while almost doubled values were found, uniformly distributed around the lesion, in SHAM (SHAM vs. treated groups ** $P < 0.01$) (Fig. 7B and C and *SI Appendix, Fig. S7A*). On the other hand, myelination (MBP), vascular ingrowth (VWF), and microglial infiltration (IBA1) seemed

not be influenced by the tested treatments (Fig. 7B and C and *SI Appendix, Fig. S6B*)

HYDROSAP and hNSCs Favor Host-Neural Regeneration in Vivo. Presence of nerve fibers positive to β III-TUB, GAP43, SMI31, GABA, and VGLUT1 markers (regardless of their source, host or donor) were analyzed in longitudinal sections of host tissue surrounding the lesions in all groups (Fig. 8). The presence of β III-TUB⁺ and GAP43⁺ fibers was significantly enhanced in both hNSC-HYDROSAP groups (β III-TUB: 1 d 0.033 ± 0.007 mm², 6 wk 0.033 ± 0.003 mm²; GAP43: 1 d 0.04 ± 0.01 mm² and 6 wk 0.043 ± 0.013 mm²), but were barely identified in the SHAM group (β III-TUB: 0.016 ± 0.001 mm²; GAP43: 0.007 ± 0.001 mm²).

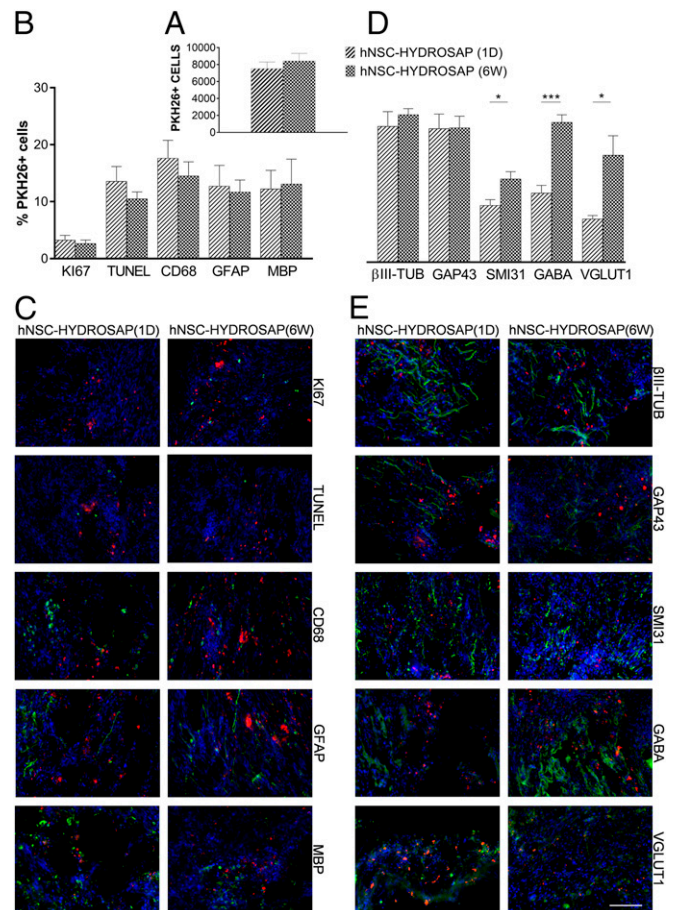


Fig. 6. HYDROSAP-transplanted hNSC engraftment in SCI. PKH26-labeled hNSCs (1.8×10^6 cells) were seeded in HYDROSAP scaffolds [hNSC-HYDROSAP(1D) and hNSC-HYDROSAP(6W)] and subsequently implanted in spinal cord hemisections ($n = 5$ per group). (A) Quantification of total number of PKH26⁺ cells per animal belonging to the same group. (B) Colocalization assessment of PKH26⁺ cells and makers of proliferation (KI67), apoptosis (Tunel), macrophage phagocytosis (CD68), and astrocytic (GFAP), myelin (MBP) differentiation. (C) Representative fields at the lesion edges (longitudinal spinal cord sections) immunostained for the above-mentioned markers. (D) Neurons were stained for β III-TUB (microtubules), GAP43 (neuronal growth-cones), SMI31 (phosphorylated neurofilament-H), GABA (γ -aminobutyric acid neurotransmitter), and VGLUT1 (glutamate transporter). Data are presented as mean \pm SEM. Significantly higher percentages of PKH26-labeled cells positive for SMI31, GABA, and VGLUT1 were detected in hNSC-HYDROSAP(6W) than in hNSC-HYDROSAP(1D) (unpaired t test, * $P < 0.05$ and *** $P < 0.001$). (E) Representative fields at the lesion edges (longitudinal spinal cord sections) immunostained for the above-mentioned markers. All markers are in green and PKH26 cells are in red. Cell nuclei were counterstained with Hoechst (blue). (Scale bar, 100 μ m for C and E.)

concerns typical of embryonic stem cells; (ii) they are already committed to nervous differentiation (i.e., do not require reprogramming); and (iii) they can be used as cellular transplants in clinical trials (46). In this work we developed and characterized a SAP-based substrate (HYDROSAP) designed to foster human GMP-grade NSC differentiation and maturation in vitro in serum-free conditions, avoiding compounds not compatible with clinics. As first application of the obtained interconnected 3D network of electrically active neural cells, we tested its neuroregenerative potential in SCI.

hNSCs were embedded in a synthetic ECM-like scaffold (pureHYDROSAP) comprising differently functionalized (with KLPGWSG and SLSVND proregenerative functional motifs) linear (LDLK)₃ (28, 29) and standard linear (LDLK)₃ SAPs, all mixed with three-branched (LDLK)₃ SAP [named Tris(LDLK)₃] (13). The selected functional motifs foster cell–matrix interaction improving NSC adhesion/viability and promote neuronal differentiation (28, 29). Furthermore, we demonstrated that when Tris(LDLK)₃ is mixed with linear (LDLK)₃, it increases the overall scaffold stiffness (13): this allowed us to decrease the final concentration of SAP in our system [below 0.5% (wt/vol)] while keeping the scaffold mechanical properties in the range of nervous tissues (100–1,000 Pa) (32), favorable to hNSC differentiation toward neuronal lineages (29). pureHYDROSAP showed elastic solid-like behavior, a typical strain-to-rupture of soft self-assembled hydrogel and presence of cross-β fibril structures. In addition, by adding NaOH, sucrose, and cell-culture medium, screening part of electrostatic repulsions (and favoring nanofiber entanglements before scaffold formation) among SAP molecules (47), to pureHYDROSAP to obtain HYDROSAP, we increased the overall viscosity of SAP solutions. hNSC-HYDROSAP was characterized in vitro for up to 10 wk to: (i) assess hNSC spreading, differentiation, and electrical activity at various time-points; (ii) detect hNSC apoptosis; (iii) track the onset of mature neuronal markers; and (iv) select the hNSC-HYDROSAP constructs showing satisfactory combination of the above points for subsequent in vivo experiments.

Densely seeded hNSCs spread and gave rise to entangled and evenly distributed cellular networks over weeks; however, no supracellular complex structure resembling any known nervous component (cortex, hippocampus, and so forth) was detected. Notably, all marker expression was evenly distributed throughout the sample slices. A negligible cytotoxicity was detected at 1 DIV, hNSC-HYDROSAP(1D); however, apoptotic cells increased at 1 wk and plateaued until 6 wk, to increase again after 8 wk in vitro. As expected, these values were significantly lower in animal-derived and growth factor-rich CULTREX-BME, but it is our opinion they can be improved in the future, for example, by loading SAP-matrices with specific neurotrophic factors. In vitro culturing revealed down-regulation of proliferative (KI67) and progenitor cell (Nestin) markers, counterbalanced by up-regulation of neuronal and glial markers. Until 2 wk in vitro, 15% of the cell population was KI67⁺, but that percentage was almost obliterated after 4 wk in culture. hNSC-HYDROSAP(1D), largely constituted by undifferentiated Nestin⁺ cells, showed a poor population of neuronal and astroglial cells, and a total absence of oligodendrocyte-tested markers. After 1 wk, seeded hNSCs underwent differentiation testified by remarkably increased percentages of neurons, astrocytes, and oligodendrocytes. However, after 4 wk, the percentage of βIII-TUB⁺ cells featured a negative trend until the end of the experiment. Reduced percentages of immature neurons could be associated with (i) progressive cell maturation, (ii) phenotype-selective reduction of cell viability, or (iii) variation of cell proliferation rate. In our case we demonstrated that long-term neural differentiation was related to neuronal maturation.

Expression of MAP2, a neuronal marker involved in dendrite stabilization during neuronal development, was weak in neuronal precursors but showed a positive trend after the expression of βIII-TUB (48), peaking at 6 wk, and with significant differences

compared with the first weeks. Similarly, GAP43, one of the earliest axon-specific markers to be expressed in neurons (49), was highly expressed at immature growing axonal terminals [~30% of neurons in hNSC-HYDROSAP(4W) and hNSC-HYDROSAP(6W)] and decreased concomitant with cell maturation [~20% in hNSC-HYDROSAP(10W)]. Neuronal differentiation was confirmed also by the expression of SMI31 phosphorylated neurofilament H, abundant in the extensive network of neurites. In vitro maturation revealed a highly enriched population of GABAergic and glutamatergic neurons. While GABA⁺ cells were highly expressed since 1 wk (~20%), VGLUT1 marker expression increased over time, from the first week (10%) up to 10 wk (~20%). The different timings in the expression of mature neuronal markers may appear to be contrasting; however, they represent different stages of neuronal differentiation and maturation (50). In addition, ChAT⁺ cells were detected since 1 wk in vitro while the presence of MBP cells was noticed at 4 wk. The conjoint presence of GABAergic, glutamatergic, and cholinergic neurons in vitro testified a good level of maturation in vitro of hNSC seeded in HYDROSAP synthetic scaffold in serum-free conditions.

Besides differentiation, electrical activity and network formation through synaptic connections are also key functional properties of neurons (51–53). Whole-cell patch-clamp recordings, used to assess electrophysiological properties of single neurons, were difficult in 3D set-ups because scaffolds may sometimes occlude the ultrafine thin glass pipette tips; thus, functional analyses of 3D cultures were mainly performed at 50- to 70-μm depth from the construct surface but, thanks also to the previously described histological results, they can be reasonably considered as representative of the whole specimens. In line with the presence of mature neurons detected in immunostainings, hNSC-differentiated cells cultured in HYDROSAP showed current densities compatible with neurons and were able to fire evoked action potentials from 4 wk in vitro until the end of experimental time frame. This finding corroborated the idea of an overall cellular maturation given by HYDROSAP, capable of culminating with the formation of active neurons in vitro. Most of the obtained results in vitro were also replicated, with a few exceptions, with CULTREX 3D, a substrate used as a positive control under identical cell culture conditions. In particular, hNSCs cultured in CULTREX-BME displayed an earlier differentiation (onset of GALC/O4⁺ cells at 1 d and percentages of MAP2⁺ and SMI31⁺ cells higher than hNSC-HYROSAP at 1 wk). Likely, CULTREX-BME enhanced hNSC differentiation and maturation because it is an animal-derived matrix rich in growth factors and cell-signaling-related proteins. Furthermore, in HYDROSAP we detected higher percentages of glutamatergic neurons than in CULTREX-BME, but this unexpected outcome should be investigated in additional studies in the near future. Nonetheless, only the characterized 3D construct, developed in serum-free conditions and obtained with fully synthetic HYDROSAP and GMP-grade hNSCs, can be potentially used for neural tissue engineering clinical therapies; however, its neuro-regenerative efficacy in vivo needed to be verified. In the chosen subacute model of surgical SCI (and usually in contusive chronic SCI), a fluid-filled cavity is still present at the time of implantation; hence, direct injections of free hNSCs (i.e., an hNSC experimental group) would have been poorly informative as, due to consistent loss of nervous tissue, transplanted cells need a physical support preventing their elution, preserving their homeostasis from the caustic post-SCI environment, coaxing their differentiation and, consequently, favoring their engraftment in vivo. Transplantation of our 3D construct derived from human pluripotent stem cells resulted in neuronal differentiation, progressive maturation and engraftment in SCI in vivo, suggesting that encapsulated cells could integrate and form functional circuits in the CNS (54).

Our combined strategy aimed to overcome the unfavorable (to both transplant engraftment and nervous regeneration) host microenvironment at the injury site in SCI by restoring a proper

milieu constituted by a functionalized ECM (scaffold) guiding the differentiation/engraftment of transplanted cells (hNSC) and also fostering the host-tissue cellular infiltration. Intriguingly, others suggested that differentiation of hNSCs into a neuronal phenotype before transplant may be a favorable strategy for in vivo cell restoration (7); hence, we also wanted to tackle the issue of the optimal differentiation status of hNSC required for best results in our in vivo model. That is why we chose hNSC-HYDROSAP(1D) and hNSC-HYDROSAP(6W). In both groups the combined treatment was capable of inducing significant locomotor improvements in treated rats, as shown by BBB. The critical role of exercise in the management of SCI is undisputed (55). Unlike BBB scoring, where an animal ambulates at a self-directed and variable speed, the treadmill apparatus uses fixed speeds. Indeed, like in many other SCI animal studies (56), we detected a beneficial effect on animal health given by exercise training in all injured animals; however, extrapolating significant data from rehabilitation sessions can be helpful but it may be still premature in this work, as a better tuning of treadmill speed to more efficiently highlight differences among the experimental groups, is recommended for future experiments. On the other hand, BBB score, a well-validated and widely adopted test, showed significant differences among treated and SHAM groups. Body weight was used as a surrogate marker of recovery following dorsal hemisection; despite its initial decrease immediately after injury, the subsequent increase well-correlated with functional recovery (57), showing that enhanced locomotor activity led to an improvement in body weight as well.

In hNSC-HYDROSAP groups transplanted hNSCs differentiated and integrated into host tissues: indeed, immunohistochemical analysis revealed abundant numbers of PKH26⁺ cells at 2 mo after treatment. Less than 15% PKH26 apoptotic cells were present while proliferating (KI67) PKH26 cells were minimal in accordance with the in vitro results. Notably, predifferentiated cells in hNSC-HYDROSAP(6W) yielded to significantly higher percentages of transplanted cells showing markers for mature neurons (SMI31, GABA, VGLUT1), suggesting a beneficial effect (in terms of differentiation) given by the pretreatment in vitro. Additionally, transplanted cells in hNSC-HYDROSAP(1D) and hNSC-HYDROSAP(6W) showed also expression (not significantly different between the two groups) of GFAP, MBP, CD68, and IBA1 markers; presence of the last two markers suggests a consistent room for improvement of the chosen immunosuppressive therapy used in our approach. Nonetheless, in terms of host-tissue response, we observed significantly decreased values of total CD68⁺ area in all treated groups if compared with SHAM, while IBA1 showed a similar trend but with less pronounced differences. These observations are in accordance with the good biocompatibility and the antiinflammatory effect of functionalized SAPs tested in SCI (27, 58). Functional recovery correlated well with data from unsaturated CSPGs and GFAP reactivity assays; similarly to Snyder's group and to our previous findings, reporting that scaffold alone may reduce glial scar formation (59), results pointed out that the HYDROSAP and hNSC-HYDROSAP groups resulted in decreased astrogliosis and increased ECM remodeling (24), both features usually associated with better nerve fibers infiltration at the lesion site (60, 61). Various studies showed that hNSCs administration in SCI can exert positive effects on neural regeneration (62, 63). Furthermore, hNSCs are used in clinical trials targeting different diseases of the CNS (46). In our case, in agreement with BBB behavioral data, we detected significantly increased values of all tested neural markers at the lesion site in both hNSC-

HYDROSAP groups (but not in HYDROSAP) if compared with SHAM, being the highest for GAP43 and β III-TUB markers, but still significant for GABAergic and glutamatergic neurons. Presumably, this was indicative of a still ongoing neural regeneration taking place at the end of the experimental time frame, which could be better addressed in future experiments with longer observation times. Instead, the greater number of mature neurons detected in cell-treated groups could be due to prolonged action of the scaffold overtime (64), promoting transplanted cell differentiation in hNSC-HYDROSAP(1D), helping to preserve the differentiation and maturation profiles achieved in vitro in hNSC-HYDROSAP(6W) and coaxing host-tissue regeneration. Indeed, even if most of the results in vivo among hNSC-HYDROSAP groups were similar, hNSC-HYDROSAP(6W) showed higher values of SMI31⁺, GABA⁺, and VGLUT1⁺ neurons than in hNSC-HYDROSAP(1D), where transplanted undifferentiated cells showed smaller percentages of SMI31⁺, GABA⁺, and VGLUT1⁺ neurons.

Finally, despite the average best performance of hNSC-HYDROSAP groups, a few significant differences with HYDROSAP were detected (e.g., CSPG degradation, caudal expression of GAP43). However, this study shows therapeutic options for hNSC manipulation and transplantation: it is our opinion that testing hNSC predifferentiated in vitro at additional different time frames and better tailoring their differentiation in vitro (and in vivo) with cytokines embedded directly into HYDROSAP (65) may largely corroborate and improve the results here described.

In the present work we deeply characterized a 3D cell culture model of densely seeded hNSCs, demonstrating the formation of an entangled network of mature and functional neural phenotypes, useful for in vitro studies. Intrigued by its translational possibilities (synthetic scaffold, GMP-hNSCs, serum-free cultures) we also demonstrated its neuroregenerative potential in vivo by testing two different levels of differentiation for hNSCs implants: this study will likely lead the way to several other tests and treatments in SCI.

Materials and Methods

A detailed description of all materials and methods used is provided in *SI Appendix, Supplementary Materials and Methods*, including hNSC cultures and PKH26 labeling, synthesis and characterization of HYDROSAP and cross-CK lamina, electrophysiology and immunofluorescence analysis, preparation of a CULTREX 3D sample, a dorsal hemisection model, rehabilitation and behavioral tests, CSPG quantification, and immunohistochemical and statistical analyses.

hNSCs. hNSCs used in this work were produced according to GMP, as dictated by the European Medical Agency guidelines, and in full accord with the WMA Declaration of Helsinki (Ethical Principles for Medical Research Involving Human Subjects). Production received formal approval and certification by the Agenzia Italiana del Farmaco, protocol aM 101/2010. Human fetal forebrain tissue specimens were collected from fetuses later than the 8th postconceptional week. Tissue procurement was approved by the Ethical Committee of Umbria's Health Institutes, and was obtained only upon written informed consent by the mother.

Animals. All in vivo procedures were carried out following protocols approved by the Institutional Animal Care and User Committee of the University of Milan-Bicocca (IACUC 445/2017-PR) and in accordance with EC guidelines (86/609/EEC) and the Italian legislation on animal experimentation (Decreto L. vo 116/92).

ACKNOWLEDGMENTS. We thank Edoardo Bolla for his help in animal care practices. Work was supported by the "Ricerca Corrente 2017–2018" funding granted by the Italian Ministry of Health; by the "5 × 1,000" voluntary contributions; by Revert; and by Vertical Onlus.

1. Lou YR, Leung AW (2018) Next generation organoids for biomedical research and applications. *Biotechnol Adv* 36:132–149.
2. Ho BX, Pek NMQ, Soh BS (2018) Disease modeling using 3D organoids derived from human induced pluripotent stem cells. *Int J Mol Sci* 19:E936.
3. Candiello J, et al. (2018) 3D heterogeneous islet organoid generation from human embryonic stem cells using a novel engineered hydrogel platform. *Biomaterials* 177:27–39.

4. Lancaster MA, et al. (2013) Cerebral organoids model human brain development and microcephaly. *Nature* 501:373–379.
5. Ogawa M, et al. (2015) Directed differentiation of cholangiocytes from human pluripotent stem cells. *Nat Biotechnol* 33:853–861.
6. Mariani J, et al. (2015) FOXG1-dependent dysregulation of GABA/glutamate neuron differentiation in autism spectrum disorders. *Cell* 162:375–390.

7. Abeyasinghe HC, et al. (2015) Pre-differentiation of human neural stem cells into GABAergic neurons prior to transplant results in greater repopulation of the damaged brain and accelerates functional recovery after transient ischemic stroke. *Stem Cell Res Ther* 6:186.
8. Zhang D, et al. (2013) Tissue-engineered cardiac patch for advanced functional maturation of human ESC-derived cardiomyocytes. *Biomaterials* 34:5813–5820.
9. Watson CL, et al. (2014) An in vivo model of human small intestine using pluripotent stem cells. *Nat Med* 20:1310–1314.
10. Li J, et al. (2018) Functional 3D human liver bud assembled from MSC-derived multiple liver cell lineages. *Cell Transplant*, 10.1177/0963689718780332.
11. Hughes CS, Postovit LM, Lajoie GA (2010) Matrigel: A complex protein mixture required for optimal growth of cell culture. *Proteomics* 10:1886–1890.
12. Pugliese R, Marchini A, Saracino GA, Gelain F (2018) Functionalization of self-assembling peptides for neural tissue engineering. *Self-Assembling Biomaterials*, eds Azevedo HS, da Silva RMP (Woodhead Publishing, Sawston, UK), pp 475–493.
13. Pugliese R, Fontana F, Marchini A, Gelain F (2018) Branched peptides integrate into self-assembled nanostructures and enhance biomechanics of peptidic hydrogels. *Acta Biomater* 66:258–271.
14. Zhao W, et al. (2017) Mechanisms responsible for the inhibitory effects of epothilone B on scar formation after spinal cord injury. *Neural Regen Res* 12:478–485.
15. Alizadeh A, et al. (2017) Neuregulin-1 positively modulates glial response and improves neurological recovery following traumatic spinal cord injury. *Glia* 65:1152–1175.
16. Levine J (2016) The reactions and role of NG2 glia in spinal cord injury. *Brain Res* 1638:199–208.
17. Gomes ED, et al. (2018) Co-transplantation of adipose tissue-derived stromal cells and olfactory ensheathing cells for spinal cord injury repair. *Stem Cells* 36:696–708.
18. Lindsay SL, et al. (2017) Human olfactory mesenchymal stromal cell transplants promote remyelination and earlier improvement in gait co-ordination after spinal cord injury. *Glia* 65:639–656.
19. Piłłiti KM, et al. (2017) Increasing human neural stem cell transplantation dose alters oligodendroglial and neuronal differentiation after spinal cord injury. *Stem Cell Rep* 8:1534–1548.
20. Fan L, et al. (2018) Directing induced pluripotent stem cell derived neural stem cell fate with a three-dimensional biomimetic hydrogel for spinal cord injury repair. *ACS Appl Mater Interfaces* 10:17742–17755.
21. Ansari S, et al. (2017) Regulation of the fate of dental-derived mesenchymal stem cells using engineered alginate-GelMA hydrogels. *J Biomed Mater Res A* 105:2957–2967.
22. López-Serrano C, et al. (2016) Effects of the post-spinal cord injury microenvironment on the differentiation capacity of human neural stem cells derived from induced pluripotent stem cells. *Cell Transplant* 25:1833–1852.
23. Gelain F, et al. (2011) Transplantation of nanostructured composite scaffolds results in the regeneration of chronically injured spinal cords. *ACS Nano* 5:227–236.
24. Cigognini D, et al. (2011) Evaluation of early and late effects into the acute spinal cord injury of an injectable functionalized self-assembling scaffold. *PLoS One* 6:e19782.
25. Zweckberger K, Ahuja CS, Liu Y, Wang J, Fehlings MG (2016) Self-assembling peptides optimize the post-traumatic milieu and synergistically enhance the effects of neural stem cell therapy after cervical spinal cord injury. *Acta Biomater* 42:77–89.
26. Caron I, et al. (2016) A new three dimensional biomimetic hydrogel to deliver factors secreted by human mesenchymal stem cells in spinal cord injury. *Biomaterials* 75:135–147.
27. Cigognini D, Silva D, Paloppi S, Gelain F (2014) Evaluation of mechanical properties and therapeutic effect of injectable self-assembling hydrogels for spinal cord injury. *J Biomed Nanotechnol* 10:309–323.
28. Gelain F, et al. (2012) New bioactive motifs and their use in functionalized self-assembling peptides for NSC differentiation and neural tissue engineering. *Nanoscale* 4:2946–2957.
29. Caprini A, et al. (2013) A novel bioactive peptide: Assessing its activity over murine neural stem cells and its potential for neural tissue engineering. *N Biotechnol* 30:552–562.
30. Horii A, Wang X, Gelain F, Zhang S (2007) Biological designer self-assembling peptide nanofiber scaffolds significantly enhance osteoblast proliferation, differentiation and 3-D migration. *PLoS One* 2:e190.
31. Cunha C, Panseri S, Villa O, Silva D, Gelain F (2011) 3D culture of adult mouse neural stem cells within functionalized self-assembling peptide scaffolds. *Int J Nanomedicine* 6:943–955.
32. Arani A, et al. (2015) Measuring the effects of aging and sex on regional brain stiffness with MR elastography in healthy older adults. *Neuroimage* 111:59–64.
33. Gelain F, et al. (2011) BMHP1-derived self-assembling peptides: Hierarchically assembled structures with self-healing propensity and potential for tissue engineering applications. *ACS Nano* 5:1845–1859.
34. Fatehullah A, Tan SH, Barker N (2016) Organoids as an in vitro model of human development and disease. *Nat Cell Biol* 18:246–254.
35. Kjell J, Olson L (2016) Rat models of spinal cord injury: From pathology to potential therapies. *Dis Model Mech* 9:1125–1137.
36. Payne SL, et al. (2018) In vitro maturation of human iPSC-derived neuroepithelial cells influences transplant survival in the stroke-injured rat brain. *Tissue Eng Part A* 24:351–360.
37. Zhao Y, Xiao Z, Chen B, Dai J (2017) The neuronal differentiation microenvironment is essential for spinal cord injury repair. *Organogenesis* 13:63–70.
38. Raspa A, Pugliese R, Maleki M, Gelain F (2016) Recent therapeutic approaches for spinal cord injury. *Biotechnol Bioeng* 113:253–259.
39. Quraishi S, Forbes LH, Andrews MR (2018) The extracellular environment of the CNS: Influence on plasticity, sprouting, and axonal regeneration after spinal cord injury. *Neural Plast* 2018:2952386.
40. Lutolf MP, Gilbert PM, Blau HM (2009) Designing materials to direct stem-cell fate. *Nature* 462:433–441.
41. Centeno EGZ, Cimarosti H, Bithell A (2018) 2D versus 3D human induced pluripotent stem cell-derived cultures for neurodegenerative disease modelling. *Mol Neurodegen* 13:27.
42. Kaushik G, Ponnusamy MP, Batra SK (2018) Concise review: Current status of three-dimensional organoids as pre-clinical models. *Stem Cells* 36:1329–1340.
43. Jo J, et al. (2016) Midbrain-like organoids from human pluripotent stem cells contain functional dopaminergic and neuromelanin-producing neurons. *Cell Stem Cell* 19:248–257.
44. Kelava I, Lancaster MA (2016) Dishing out mini-brains: Current progress and future prospects in brain organoid research. *Dev Biol* 420:199–209.
45. Pugliese R, Gelain F (2017) Peptidic biomaterials: From self-assembling to regenerative medicine. *Trends Biotechnol* 35:145–158.
46. Mazzini L, et al. (2015) Human neural stem cell transplantation in ALS: Initial results from a phase I trial. *J Transl Med* 13:17.
47. Caplan MR, Moore PN, Zhang S, Kamm RD, Lauffenburger DA (2000) Self-assembly of a beta-sheet protein governed by relief of electrostatic repulsion relative to van der Waals attraction. *Biomacromolecules* 1:627–631.
48. Cáceres A, Banker GA, Binder L (1986) Immunocytochemical localization of tubulin and microtubule-associated protein 2 during the development of hippocampal neurons in culture. *J Neurosci* 6:714–722.
49. Morita S, Miyata S (2013) Synaptic localization of growth-associated protein 43 in cultured hippocampal neurons during synaptogenesis. *Cell Biochem Funct* 31:400–411.
50. Garner CC, Matus A (1988) Different forms of microtubule-associated protein 2 are encoded by separate mRNA transcripts. *J Cell Biol* 106:779–783.
51. Otani T, Marchetto MC, Gage FH, Simons BD, Livesey FJ (2016) 2D and 3D stem cell models of primate cortical development identify species-specific differences in progenitor behavior contributing to brain size. *Cell Stem Cell* 18:467–480.
52. Piper DR, Mujtaba T, Rao MS, Lucero MT (2000) Immunocytochemical and physiological characterization of a population of cultured human neural precursors. *J Neurophysiol* 84:534–548.
53. Bardy C, et al. (2015) Neuronal medium that supports basic synaptic functions and activity of human neurons in vitro. *Proc Natl Acad Sci USA* 112:E2725–E2734.
54. Mansour AA, et al. (2018) An in vivo model of functional and vascularized human brain organoids. *Nat Biotechnol* 36:432–441.
55. Ginis KA, et al. (2010) Leisure time physical activity in a population-based sample of people with spinal cord injury part I: Demographic and injury-related correlates. *Arch Phys Med Rehabil* 91:722–728.
56. Battistuzzo CR, Callister RJ, Callister R, Galea MP (2012) A systematic review of exercise training to promote locomotor recovery in animal models of spinal cord injury. *J Neurotrauma* 29:1600–1613.
57. Zhang Y, et al. (2007) Observation of locomotor functional recovery in adult complete spinal rats with BWSTT using semiquantitative and qualitative methods. *Spinal Cord* 45:496–501.
58. Raspa A, et al. (2016) A biocompatibility study of new nanofibrous scaffolds for nervous system regeneration. *Nanoscale* 8:253–265.
59. Teng YD, et al. (2002) Functional recovery following traumatic spinal cord injury mediated by a unique polymer scaffold seeded with neural stem cells. *Proc Natl Acad Sci USA* 99:3024–3029.
60. Liu Y, et al. (2013) A self-assembling peptide reduces glial scarring, attenuates post-traumatic inflammation and promotes neurological recovery following spinal cord injury. *Acta Biomater* 9:8075–8088.
61. Amemori T, et al. (2015) Comparison of intraspinal and intrathecal implantation of induced pluripotent stem cell-derived neural precursors for the treatment of spinal cord injury in rats. *Stem Cell Res Ther* 6:257.
62. Rosenzweig ES, et al. (2018) Restorative effects of human neural stem cell grafts on the primate spinal cord. *Nat Med* 24:484–490.
63. Wilcox JT, Satkunendrarajah K, Zuccato JA, Nassiri F, Fehlings MG (2014) Neural precursor cell transplantation enhances functional recovery and reduces astrogliosis in bilateral compressive/contusive cervical spinal cord injury. *Stem Cells Transl Med* 3:1148–1159.
64. Yao ZA, et al. (2018) Efficacy of chitosan and sodium alginate scaffolds for repair of spinal cord injury in rats. *Neural Regen Res* 13:502–509.
65. Gelain F, Unsworth LD, Zhang S (2010) Slow and sustained release of active cytokines from self-assembling peptide scaffolds. *J Control Release* 145:231–239.